^{58}Co: Structure of an odd-odd nucleus in the pf shell

M. A. G. Silveira, N. H. Medina, J. R. B. Oliveira, J. A. Alcántara-Núñez, E. W. Cybulska, H. Dias, M. N. Rao, R. V. Ribas, W. A. Seale, and K. T. Wiedemann
Instituto de Física, Universidade de São Paulo, São Paulo, SP, Brazil

B. A. Brown
Department of Physics and Astronomy, Michigan State University, East Lansing, Michigan 48824, USA and National Superconducting Cyclotron Laboratory, Michigan State University, East Lansing, MI 48824

M. Honma
Center for Mathematical Sciences, University of Aizu, Tsuruga, Ikki-machi, Aizu-Wakamatsu, Fukushima 965-8580, Japan

T. Mizusaki
Institute of Natural Sciences, Senshu University, Higashimita, Tama, Kawasaki, Kanagawa 214-8580, Japan

T. Otsuka
Department of Physics and Astronomy, University of Tokyo, Hongo, Tokyo 113-0033, Japan and RIKEN, Hirosawa, Wako-shi, Saitama 351-0198, Japan

(Received 2 February 2006; revised manuscript received 16 August 2006; published 18 December 2006)

High-spin states in the odd-odd ^{58}Co nucleus have been studied with the fusion-evaporation reaction ^{51}V (^{10}B, $p2n$) using the γ-spectrometer Saci-Perere. Thirty-six new excited states up to spin 11^+ and an excitation energy of 8.0 MeV have been observed, which are connected by 46 γ-ray transitions. Transition probabilities for 14 excited states were measured through the Doppler-shift attenuation method. The results are compared with shell-model calculations using the GXPF1 effective interaction, developed for use in the pf shell. These results were interpreted by considering particle-hole excitations with respect to the doubly magic $N = Z = 28$ core.

DOI: 10.1103/PhysRevC.74.064312 PACS number(s): 27.40.+z, 23.20.Lv, 21.10.Tg, 21.60.Cs

I. INTRODUCTION

The problem of describing microscopically the nuclear structure of a large number of active and interacting nucleons is a challenge for both nuclear structure models and the effective interactions. The effective interactions between nucleons can be derived, in principle, from the free nucleon-nucleon interaction and, in fact, such a microscopic interaction was proposed in 1968 by Kuo and Brown (KB) for pf shell nuclei [1]. When applied to many-valence particles in nuclei such as ^{48}Ca the KB interaction fails to reproduce the observed spectra [2,3]. It is found that better agreement with spectra and binding energies can be obtained when empirical two-body matrix elements are used. The major change from KB involves about 10 monopole linear combinations of two-body matrix elements [2–4]. However, some modification of up to 70 linear combinations of matrix elements is needed to obtain optimal agreement with spectra over the mass region $A = 47 - 66$ [5]. Another interaction, with minor modifications in its monopole term, has been successfully used to describe lighter pf-shell nuclei, in what is usually called the large-scale shell model [3–5]. Such effective interactions can be modified, for practical use, to carry out an empirical fit to a sufficiently large quantity of experimental energies.

The shell gap at $N = Z = 28$ is due to the spin-orbit lowering of the $f_{7/2}$ orbital and is rather small, so that the particle-hole excitation across the gap has relatively low energies [6–10]. In many shell-model calculations, ^{56}Ni has often been assumed as an inert core. However, it has been shown that, with this rather soft core [11], the closed-shell model for the magic number 28 provides a very limited description, especially for nuclei near N or $Z = 28$ semimagic. Recently, a new effective interaction called GXPF1 for the fp nuclei has been proposed [5]. The semimagic structure was successfully described for N or $Z = 28$ nuclei, ^{53}Mn, ^{54}Fe, ^{55}Co, and ^{56,57,58,59}Ni, by allowing the existence of significant core excitations in low-lying nonyrast states as well as in high-spin yrast states [10]. The results for $N = Z$ odd-odd nuclei, ^{54}Co [10] and ^{58}Cu [9], also confirm the reliability of the GXPF1 interaction [10]. In [6] the ^{56}Co nucleus was studied with a heavy-ion reaction using the γ array NORDBALL. The level scheme was interpreted in the frame of the shell model BY allowing one, two, and three particle-hole excitations with respect to the doubly magic $N = Z = 28$ core, resulting in a fairly good agreement. The high-spin structure of ^{57}Co nucleus was studied up to an excitation energy of 16 MeV at a spin of 17–18$\hbar$ in an experiment performed using the γ array GAMMASPHERE [12]. In this case, the shell-model calculations were performed with the FPD6 residual interaction [13], which allowed a rather good description for the excited states. It is now important to analyze the wave functions and examine electromagnetic properties to further test the reliability of the GXPF1 interaction for more

 ©2006 The American Physical Society

complex nuclei. The nuclear structure of the ^{58}Co nucleus with 27 protons is a very stringent test for predictions of the shell model using this new effective interaction.

This work presents new experimental results on excited states of ^{58}Co, thus enriching the systematics of the nuclear structure along the $N = 31$ chain. This nucleus has three particles and one hole relative to the doubly magic $N = Z = 28$ core and has been studied so far with proton- and α-particle-induced reactions [14–16], populating excited states up to spin 6^+, so very little was known regarding its high-spin structure. In the present study, the level scheme of ^{58}Co has been extended to an excitation energy of 8.0 MeV and spin 11^+. Lifetimes of 14 excited states were measured with the Doppler-shift attenuation method (DSAM) standard analysis. The properties of the observed excited states were interpreted with the large-scale shell model by using the GXPF1 residual interaction with a valence space and considering excitations of up to eight particles in the full pf shell. Some preliminary results from this work were published in Refs. [17,18].

II. EXPERIMENTAL PROCEDURES

^{58}Co excited nuclei were produced by the fusion-evaporation reaction ^{51}V (^{10}B, $p2n$), using both thin and thick targets. The ^{10}B beam was provided by the 8UD Pelletron tandem accelerator of the University of São Paulo. In both experiments, $\gamma\gamma$-charged particle coincidences were measured with the Saci-Pererê γ-ray spectrometer. SACI (*Sistema Ancilar de Cintiladores*) [19] is a 4π charged-particle system consisting of 11 plastic phoswich scintillator $\triangle E$-E telescopes. The charged-particle detectors were screened against the scattered heavy ions with three Al foils of 3.0 mg/cm^2. Pererê (*Pequeno Espectrômetro de Radiação Eletromagnética com Rejeição de Espalhamento*) [20] is a γ-array spectrometer composed of four GeHP detectors with BGO Compton shields (with two detectors being Ortec GMX of about 20% efficiency and the other two Canberra REGe of 60% efficiency). Two of these detectors were placed at 37° and the other two at 101° with respect to the beam direction. The total photopeak efficiency of the system is about 0.5% at 1.3 MeV. In the thin target experiment the nuclei were populated at 33 MeV bombarding energy. The thin target consisted of a stack of three self-supporting natural ^{51}V foils of approximately 200 μg/cm^2 each. A total of 48×10^6 Compton-suppressed γ-γ events was collected and registered on the hard disk of a PC. The data have been Doppler corrected and sorted into symmetrized $\gamma\gamma$, α-gated, and proton-gated $\gamma\gamma$ matrices with 9.4. $\times 10^7$, 2.5×10^6, and 10.5×10^6 counts, respectively. In the thick target experiment the reaction was performed at 36 MeV bombarding energy. The target consisted of a 770 μg/cm^2 foil on a Pb backing. A total of 20×10^6 Compton-suppressed γ-γ events were collected. Events were collected when at least two HPGe detectors fired in coincidence. γ-ray energy and efficiency calibrations were made with ^{56}Co,^{133}Ba, and ^{152}Eu sources. Background-subtracted spectra generated from those matrices were used to construct the level scheme of ^{58}Co. Those matrices were analyzed using the UPAK [21], GASPWARE [22], and RADWARE [23] spectrum analysis codes. The γ-ray transitions belonging to ^{58}Co were identified by setting gates on charged particle fold 1p. The γ rays from ^{57}Co (corresponding to the p3n channel), which is the main contaminant channel in the 1p-gated spectra, were identified from previous work [12]. In Fig. 1 the γ-ray spectrum gated on the 321-keV low-lying transition of the ^{58}Co nucleus, and on protons detected by

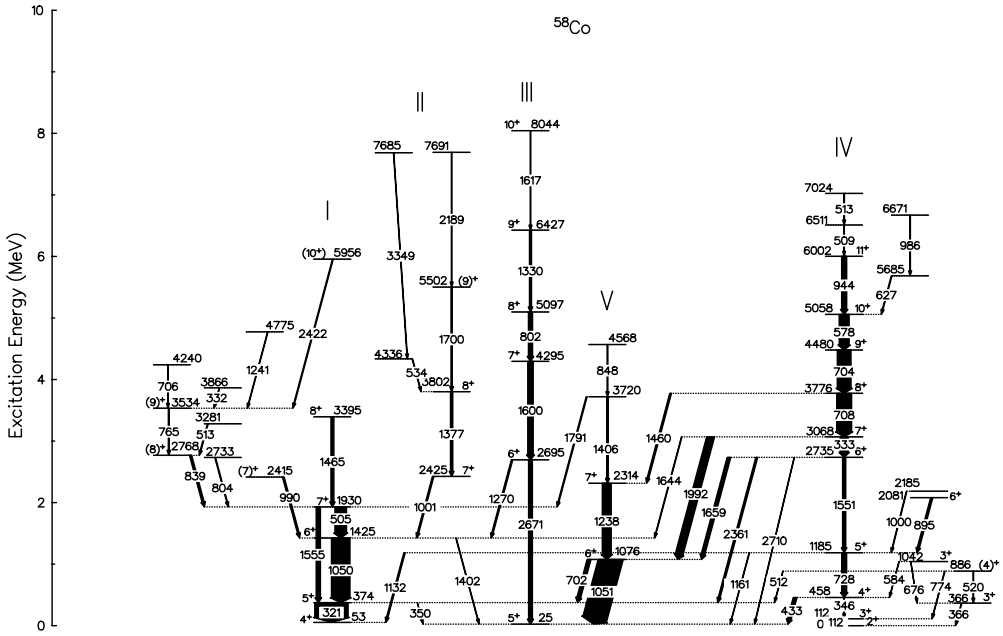

FIG. 1. γ-ray spectrum from the ^{10}B on ^{51}V (thin target experiment at $E = 33$ MeV) gated on the 321-keV low-lying transition of the ^{58}Co nucleus, and on protons detected by the SACI array. The γ rays, with energy indicated in keV, were assigned to the ^{58}Co nucleus. The symbol *refer to the ^{57}Co γ-ray lines.

the SACI array, is shown. The assignment of the spins and parities to the ^{58}Co levels was based on DCO (directional correlation from oriented states) ratios, extracted from the thin target experimental data. For this purpose, a $\gamma\gamma$ matrix was constructed by sorting the data from the two detectors, each positioned at 37° and 101°. Gates were set on each axis on several strong dipole transitions and the intensity of other transitions observed in the two spectra has been extracted. The theoretical DCO ratio was calculated with the CORR program [22]. The theoretical DCO ratios

$$R_{\mathrm{DCO}} = \frac{I_\gamma(\gamma_1 \text{ at } 37^\circ;\ \text{gated with } \gamma_2 \text{ at } 101^\circ)}{I_\gamma(\gamma_1 \text{ at } 101^\circ;\ \text{gated with } \gamma_2 \text{ at } 37^\circ)},$$

which are obtained for the present geometry, are $R_{\mathrm{DCO}} = 1.0$ for quadrupole transitions and $R_{\mathrm{DCO}} = 0.49$ for pure dipole transitions ($\Delta I = 1$), with intermediate values for moderately positive mixing ratios $\delta(E2/M1)$, when gating on a stretched quadrupole transition. It should be noted that $\Delta I = 0$ transitions could give DCO ratios between 1.1 (pure dipole) and 0.44 (large mixing ratios). In our case it was only possible to set an adequate gate on a previously determined dipole transition with known mixing ratios δ, $-0.050(25)$ and $-0.109(45)$, for 321.37(4) keV and 433.15(6) keV, respectively [24]. The resulting experimental R_{DCO} has to be multiplied by the R_{DCO} of the gating transition, which is calculated using the known δ values, to obtain the value corresponding to that of a quadrupole gate. Hence, the experimental R_{DCOq} is obtained from

$$R_{\mathrm{DCOq}} = R_{\mathrm{DCO}} \times R_{\mathrm{DCO\,gate}}.$$

III. THE LEVEL SCHEME

A level scheme extending up to an excitation energy of about 8.0 MeV and spin $I = 11^+$ has been proposed (see Fig. 2), based on the coincidence relationships, intensity balances on each level, and energy sums from different paths, using the 1p-gated matrix. Several cascades at high excitation energy show a complex level structure. We have found 46 new γ transitions depopulating 36 new excited states that were organized in five main sequences. We confirmed 17 known transition [24] energies, most of them within ± 0.5 keV. The excitation energies are referred to the previously known 2^+ ground state. The γ-ray energies and relative intensities of the transitions assigned to ^{58}Co, the DCO ratios, and the resulting spin and parity assignments are given in Tables I and II. The width of the arrows in Fig. 2 is proportional to the transition intensity as seen in the thin target experiment studied here. The transition relative intensities have been deduced from coincidence spectra. The proposed spin assignments will be discussed in the following.

In analyzing the data with RADWARE [23], the level scheme has been built up by reducing the mean-square error and attempting to eliminate inconsistencies in the predicted gate spectra. In Fig. 1 γ rays in coincidence belonging to sequences I, II, and III are shown. Figure 3 presents the γ-ray spectrum in coincidence with the 1992-keV transition, which connects sequences IV and V. In Fig. 4 the sum of the γ-ray spectra in coincidence with the 578- and 944-keV gates is shown. This spectrum shows clearly the γ rays connecting sequences IV and V. Several transitions in the proposed level scheme have similar energies. The known levels, at 1425 and 1076 keV, assigned $I^\pi = 6^+$, are depopulated with transitions 1050.37(5) and 1050.9(1) keV, respectively. The 1076-keV level, positioned in sequence V, is depopulated also by the 702-keV transition, already known from the literature. In sequence IV there are two γ rays with energies of 704 and 708 keV in coincidence with this 702-keV transition. In this work we have found only one transition with $\Delta I = 2$ quadrupole character through the DCO technique, namely 1554.7(5) keV, connecting the 1930-keV level, assigned $I^\pi = 7^+$, and the 374-keV level, assigned $I^\pi = 5^+$. All the other transitions were of dipole character with the spin increasing as the level energy is increased, with two exceptions, the

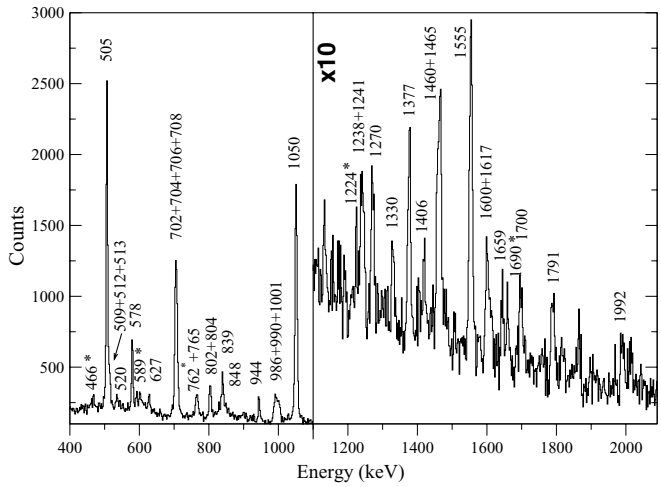

FIG. 2. The partial level scheme of ^{58}Co obtained from the present work.

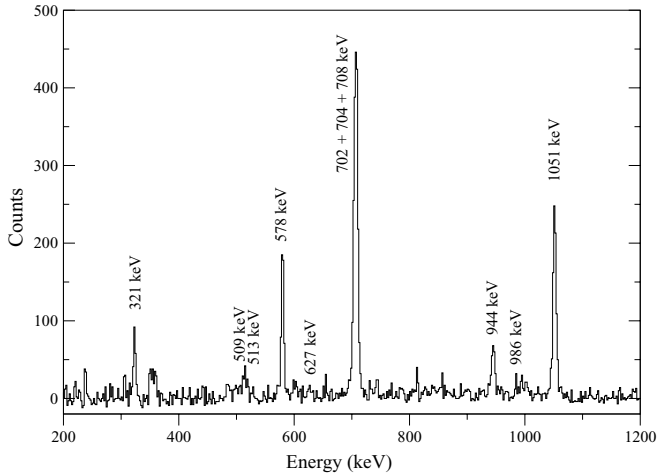

FIG. 3. γ-ray spectrum from the ^{10}B on ^{51}V (thin target experiment at $E = 33$ MeV) gated on the 1992-keV low-lying transition of the ^{58}Co nucleus, and on protons detected by the SACI array. These γ rays were assigned to the ^{58}Co nucleus.

TABLE I. γ-ray transitions assigned to ^{58}Co. The transition energy (E_γ), initial and final spin, the initial level energy (E_i), the intensity of the transition (I_γ), and the RDCOq values are present.

E_γ (keV)	E_i (keV)	E_f (keV)	$J_i \rightarrow J_f$	RDCOq	I_γ
111.9(1)	111.9(4)	0	$3^+ \rightarrow 2^+$[a]		>5
321.37(4)	374.3(9)	52.9(9)	$5^+ \rightarrow 4^+$[a]	0.458[b]	>180
332.0(2)	3866(2)	3534(1)			2.6(3)
333.06(4)	3068.2(9)	2735.2(9)	$7^+ \rightarrow 6^+$	0.40(9)	43(2)
345.9(2)	457.9(8)	24.8(9)	$4^+ \rightarrow 3^+$[a]		2.1(2)
349.70(14)	374.3(9)	24.8(9)	$5^+ \rightarrow 5^+$[a]	0.59(18)[f]	1.01(6)
366.5(3)	366.3(9)	0	$3^+ \rightarrow 2^+$[a]		>3
433.15(6)	457.9(8)	24.8(9)	$4^+ \rightarrow 5^+$[a]	0.41[b]	20(2)
505.13(5)	1929.8(9)	1424.7(9)	$7^+ \rightarrow 6^+$[a]	0.44(3)	62(2)
509.0(4)	6511(2)	6002(1)			2.1(3)
512.0(4)	886(1)	374.3(9)	$(4)^+ \rightarrow 5^+$[a]		2.1(4)
512.6(2)	3281(1)	2768(1)			4.7(4)
513.2(3)	7024(2)	6511(2)			3.0(3)
520.3(3)	886(1)	366.3(9)	$(4)^+ \rightarrow 3^+$[a]		2.5(3)
533.6(3)	4336(2)	3802(2)			2.7(3)
578.35(4)	5058(1)	4480(1)	$10^+ \rightarrow 9^+$	0.57(6)	54(2)
584.6(8)	1042(3)	457.9(8)	$3^+ \rightarrow 4^+$[a]		1.5(4)
627.1(2)	5685(1)	5058(1)			3.7(3)
675(1)	1042(3)	366.3(9)	$3^+ \rightarrow 3^+$[a]		0.6(3)
702.1(2)[c]	1076.0(9)	374.3(9)	$6^+ \rightarrow 5^+$[a]	0.52(6)[i]	20(1)
704.0(1)[d]	4480(1)	3775.7(9)	$9^+ \rightarrow 8^+$	0.52(6)[i]	74(3)
706.1(5)	4240(3)	3534(1)			2.7(5)
707.53(5)	3775.7(9)	3068.2(9)	$8^+ \rightarrow 7^+$	0.50(5)	80(3)
727.63(7)	1185.3(9)	457.9(8)	$5^+ \rightarrow 4^+$[a]	0.38(3)	27(1)
765.3(2)	3534(1)	2768(1)	$(9)^+ \rightarrow (8)^+$	0.45(5)	5.0(4)
774.1(3)	866(1)	111.9(4)	$(4)^+ \rightarrow 3^+$[a]		2.6(3)
802.3(1)	3498(1)	2695(1)	$7^+ \rightarrow 6^+$	0.54(7)	22(2)
803.7(1)	2733(2)	1929.8(9)			4.1(5)
838.6(1)	2768(1)	1929.8(9)	$(8)^+ \rightarrow 7^+$	0.36(4)	11.5(6)
848.2(5)	4568(2)	3720(2)			4.1(6)
895.3(2)	2081(1)	1185.3(9)	$(6)^+ \rightarrow 5^+$	0.34(5)	11.5(8)
943.95(7)	6002(1)	5058(1)	$11^+ \rightarrow 10^+$	0.30(5)	27(1)
985.9(4)	6671(2)	5685(1)			3.3(3)
990.4(3)	2415(2)	1424.7(9)	$(7)^+ \rightarrow 6^+$	0.38(6)	9.1(7)
999.6(7)	2185(5)	1185.3(9)			2.9(6)
1000.7(2)	2425(1)	1425(1)	$7^+ \rightarrow 6^+$	0.32(8)	7.7(7)
1050.37(5)	1424.7(9)	374.3(9)	$6^+ \rightarrow 5^+$[a]	0.47(3)	100(4)
1050.9(1)	1076.0(9)	24.8(9)	$6^+ \rightarrow 5^+$	0.31(6)[l]	131(13)
1131.9(4)	1185.3(9)	52.9(9)	$5^+ \rightarrow 4^+$[a]		7.3(8)
1161(1)	1185.3(9)	24.8(9)	$5^+ \rightarrow 5^+$[a]		2.5(7)
1237.6(1)	2314(1)	1076.0(9)	$7^+ \rightarrow 6^+$	0.46(9)	48(3)
1241.2(6)	4775(3)	3534(1)			2.6(4)
1270.3(3)	2695(1)	1425(1)	$6^+ \rightarrow 6^+$		7.6(8)
1329.6(2)	6427(2)	5097(1)	$9^+ \rightarrow 8^+$	0.38(8)[g]	10.9(8)
1376.9(2)	3802(2)	2425(1)	$8^+ \rightarrow 7^+$	0.64(9)	12.3(8)
1402(2)	1424.7(9)	24.8(9)	$6^+ \rightarrow 5^+$[a]	0.59(11)[e]	2.7(11)
1406.2(5)	3720(2)	2314(1)			8.4(9)
1460.5(3)	3775.7(9)	2314(1)	$8^+ \rightarrow 7^+$	0.39(5)	9.0(6)
1464.8(2)	3394.6(12)	1929.8(9)	$8^+ \rightarrow 7^+$	0.59(8)	15.8(8)
1550.7(1)	2735.2(9)	1185.3(9)	$6^+ \rightarrow 5^+$	0.47(5)	17(1)
1554.7(5)	1929.8(9)	374.3(9)	$7^+ \rightarrow 5^+$	0.75(8)	23(1)
1599.8(1)	5097(1)	3498(1)	$8^+ \rightarrow 7^+$	0.38(7)[h]	29(1)
1617.1(7)	8044(3)	6427(2)	$10^+ \rightarrow 9^+$	0.54(12)[g]	3.0(5)
1644.2(6)	3068.2(9)	1425(1)	$7^+ \rightarrow 6^+$		3.1(4)

TABLE I. *(Continued.)*

E_γ (keV)	E_i (keV)	E_f (keV)	$J_i \rightarrow J_f$	RDCOq	I_γ
1659.2(1)	2735.2(9)	1076.0(9)	$6^+ \rightarrow 6^+$	0.39(6)[j]	19(1)
1699.8(3)	5502(2)	3802(2)	$(9)^+ \rightarrow 8^+$	0.25(13)	6.7(6)
1790.7(4)	3720(2)	1929.8(9)			5.1(5)
1991.9(1)	3068.2(9)	1076.0(9)	$7^+ \rightarrow 6^+$	0.52(9)[i]	42(2)
2189.4(7)	7691(4)	5502(2)			2.7(4)
2361.0(2)	2735.2(9)	374.3(9)	$6^+ \rightarrow 5^+$	0.52(7)	9.9(6)
2422.2(4)	5956(2)	3534(1)	$(10)^+ \rightarrow 9^+$	0.68(13)	4.4(4)
2670.7(3)	2695(1)	24.8(9)	$6^+ \rightarrow 5^+$	0.37(8)[g]	21(3)
2710(1)	2735.2(9)	24.8(9)	$6^+ \rightarrow 5^+$	0.45(10)[k]	2.0(4)
3349.3(9)	7685(4)	4336(2)			2.1(3)

[a]Known transition [24], observed in this work.
[b]Reference [24] and program CORR.
[c]Contamination from 704.0(1)-keV transition.
[d]Contamination from 702.1(2)-keV transition.
[e]505.13(5)-keV gated transition.
[f]1050.37(5)-keV gated transition.
[g]1599.8(1)-keV gated transition.
[h]802.3(1)-keV gated transition.
[i]578.35(4)-kev gated transition.
[j]1050.9(1)-keV gated transition.
[k]333.06(4)-keV gated transition.
[l]1659.2(1)-keV gated transition.

1659-keV transition connecting the level at 2735 keV with the level at 1076 keV, and the 1270-keV transition connecting the level at 2695 keV with the level at 1425 keV. All these levels were assigned as $I^\pi = 6^+$.

IV. LIFETIME MEASUREMENTS

To allow the lifetime analysis, the thick target experimental data were sorted into two $\gamma\gamma$ matrices having on the first

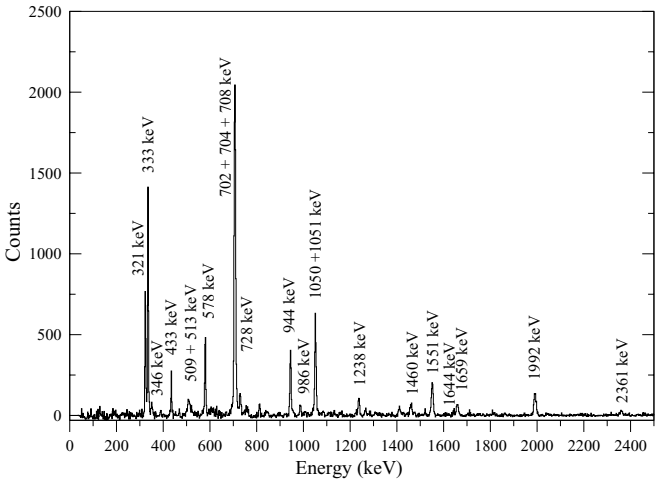

FIG. 4. γ-ray spectrum from the ^{10}B on ^{51}V (thin target experiment at $E = 33$ MeV) gated on the sum of 578- and 944-keV low-lying transitions of the ^{58}Co nucleus, and on protons detected by the SACI array. These γ rays were assigned to the ^{58}Co nucleus.

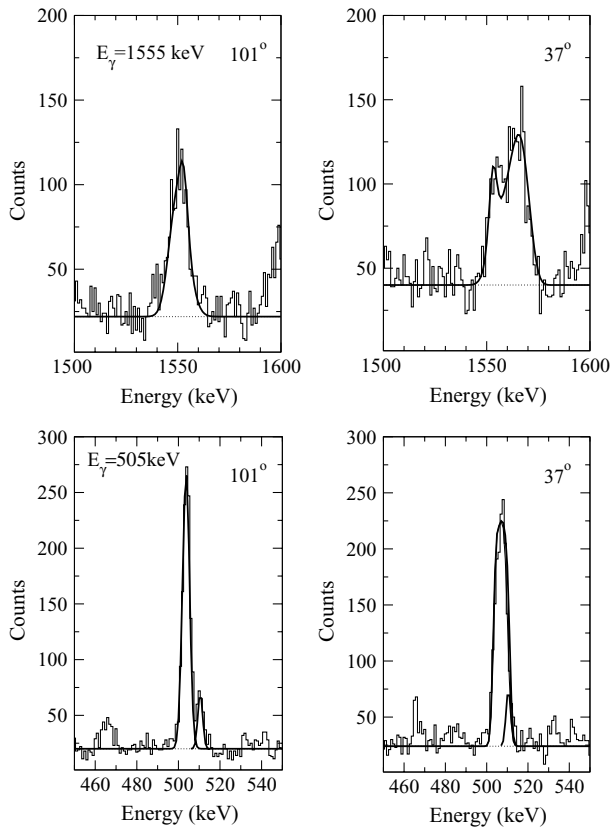

FIG. 5. Line-shape analysis for the $7^+ \rightarrow 5^+$ 1555-keV (top) and $7^+ \rightarrow 6^+$ 505-keV (bottom) transitions, observed at 101° and 37°, with a gate at 321 keV.

TABLE II. γ-ray transitions assigned to ^{58}Co, experimental and theoretical excitation energies, spin-parity, experimental and theoretical branching ratios, experimental and theoretical half-lives, and experimental theoretical reduced (BM1) values.

E_γ (keV)	E_{exp} (keV)	E_{th} (keV)	J_i	J_f	BR_{exp} (%)	BR^a_{NDS} (%)	BR_{th} (%)	τ_{exp} (ps)	τ_{th} (ps)	$B(M1)^e_{exp}$ (μ_N^2)	$B(M1)_{th}$ (μ_N^2)
	0[a]	46	2_1								
	24.95(6)[a]	0	5_1								
28.30(15)[a]	53.15(7)[a]	110	4_1	5_1		43(5)	100				
52.96(13)[a]				2_1		100	0				
253.39(24)[a]	365.66(7)[a]	340	3_2	3_1		0.9(2)					
312.39(16)[a]				2_1		100(3)	100				
321.37(4)	374.3(9)	420	5_2	4_1	100	100	100	>1	2.6	<1.7	0.63
349.7(1)				5_1	0.60(4)	6.1(2)	16			<0.01	0.04
345.9(2)	457.9(8)	395	4_2	3_1	10(1)	19.5(8)	1	>1	2.5	<0.22	0.10
433.15(6)				5_1	100(10)	100(4)	100			<0.57	0.36
91.63(27)[a]				3_2		1.5(1)	1			<0.90	1.2
519.90(14)[a]	886(1)	1037	4_3	3_2		46(3)	31				
773.93(12)[a]				3_1		100(4)	100				
832.92(31)[a]				4_1		12(1)					
860.8(5)[a]				5_1		29(3)	3				
				2_1			3				
584.6(8)	1042(3)	1124	3_3	4_2	100(27)	100(5)	45				
675.1(2)				3_2	40(20)	51(5)					
1039.80(25)[a]				2_1		66(9)	100				
				4_1			79				
1050.9(1)	1076.0(9)	1081	6_1	5_1	100(10)		100	<0.1	0.12	>0.42	0.38
702.1(2)				5_2	15(1)	100	10			>0.220.22	0.14
727.63(7)	1185.3(9)	1293	5_3	4_2	100(1)	100(4)	100	0.14(2)[b]	0.10	0.76(11)	0.40
1131.9(4)				4_1	27(3)	30(3)	48			0.055(9)	0.09
1161(1)				5_1	9(2)	15(2)	32			0.018(5)	0.04
				3_1	<5		2				
987.90(16)[a]	1353.47(13)[a]	1353	2_5	3_2		100(14)	100				
1241.53(20)[a]				3_1		42(10)	37				
1353.5(4)[a]				4_1		35(8)	2				
1050.37(5)	1424.7(9)	1522	6_2	5_2	100(4)	100(11)	100	0.11(3)	0.09	0.43(11)	0.35
1402(2)				5_1	3(1)	11.6(8)	31			0.005(2)	0.04
				4_1	<3		4				
505.13(5)	1929.8(9)	1988	7_1	6_2	100(3)		100	0.40(4)[c]	0.55	0.81(9)	0.77
				6_1	<4		3				
1554.7(5)				5_2	37(2)		29			d	d
1237.6(1)	2314(1)	2292	7_2	6_1	100(6)		40	$0.23^{+0.08}_{-0.10}$	0.34	$0.13^{+0.05}_{-0.06}$	0.02
				5_1	<8		100				
				5_2			23				
1550.7(1)	2735.2(9)	2209	6_3	5_3	88(5)		100	0.25(10)	0.08	0.021(8)	0.48
1659.2(1)				6_1	100(6)		0.4			0.020(8)	0.008
2361.0(2)				5_2	51(3)		19			0.0035(14)	0.007
2710(1)				5_1	10(2)		65			0.0005(2)	0.013
				4_1			3				
				4_2			8				
				6_2			3				
333.06(4)	3068.2(9)	3008	7_4	6_3	100(5)		49	$0.11^{+0.01}_{-0.04}$	0.05	$6.8^{+0.6}_{-2.5}$	0.36
1644.2(6)				6_2	7(1)		100			$0.0018^{+0.0003}_{-0.0007}$	0.11
1991.9(1)				6_1	98(5)		85			$0.031^{+0.011}_{-0.003}$	0.04
				5_1	<2		70				
				6_4			6				
1464.8(2)	3395(1)	3473	8_1	7_1	100(5)		100	0.10(6)	0.03	0.18(11)	0.45
				6_2	<5		6				
				7_3			16				
				6_1			3				
1406.2(4)	3720(2)	3682	(8_2)	7_3	100(11)		100				

TABLE II. *(Continued.)*

E_γ (keV)	$E_{\rm exp}$ (keV)	$E_{\rm th}$ (keV)	J_i	J_f	$BR_{\rm exp}$ (%)	$BR^{\rm a}_{\rm NDS}$ (%)	$BR_{\rm th}$ (%)	$\tau_{\rm exp}$ (ps)	$\tau_{\rm th}$ (ps)	$B(M1)^{\rm e}_{\rm exp}$ (μ_N^2)	$B(M1)_{\rm th}$ (μ_N^2)
1790.7(4)				7_1	61(6)		67				
				6_1	<6		21				
				7_2			15				
				6_3			3				
707.53(5)	3775.7(9)	3858	8_3	7_4	100(4)		0.04	0.11(1)	0.06	1.29(12)	0.0002
1460.5(3)				7_2	11(1)		100			0.0017(2)	0.15
				7_3	<2		10				
				7_1			6				
				6_2			15				
				6_1			20				
704.0(1)	4480(1)		9	8_3	100			0.11(1)		1.47(13)	
578.35(4)	5058(1)		10	9	100			0.136(14)		2.14(22)	
943.95(7)	6002(1)		11	10	100			0.090(9)		0.74(7)	

[a]From Ref. [24].
[b]$\tau = 0.20^{+0.09}_{-0.06}$; $\tau = 0.24^{+0.11}_{-0.07}$, Ref. [24].
[c]Weighted mean between values found for 1555- and 505-keV transitions.
[d]$B(E2)_{\rm exp} = 61(7)\ e^2\ {\rm fm}^4$; $B(E2)_{\rm th} = 34\ e^2\ {\rm fm}^4$.
[e]The $B(M1)_{\rm exp}$ values were extracted by assuming $\delta = 0$.

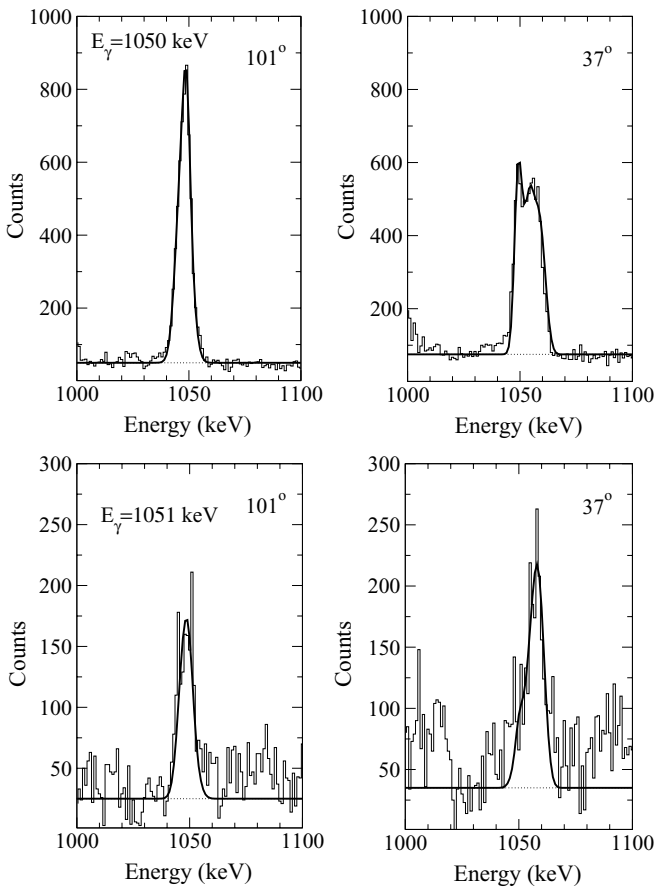

FIG. 6. Line-shape analysis for the $6^+ \rightarrow 5^+$ 1050-keV transition, depopulating the 1425-keV state, with a gate at 321 keV (top), and the $6^+ \rightarrow 5^+$ 1051-keV transition, depopulating the 1076-keV state, with a gate at 1238 keV (bottom), both observed at 101° and 37°.

axis the detectors at 37° or 101°, respectively, and on the second axis any of the other three detectors. We used the LINESHAPE code to extract the lifetimes of the excited states [25]. This code includes the recoil spread from particle emission [26] and describes the nuclear stopping power according to the Lindhard, Scharff and Schiott theory [27] using the approach of Ref. [28]. The Northcliffe-Schilling parametrization, corrected for atomic shell effects, for the electronic stopping power was adopted [29]. The history of each event was fully randomized and a statistical distribution was created for the projection of the recoil velocity along the direction of the detected γ ray as a function of time. The line shape of a transition was obtained by averaging the distribution over the transition decay curve and then folding it over the detector energy resolution. Values for 14 excited levels were determined from the analysis of pronounced line

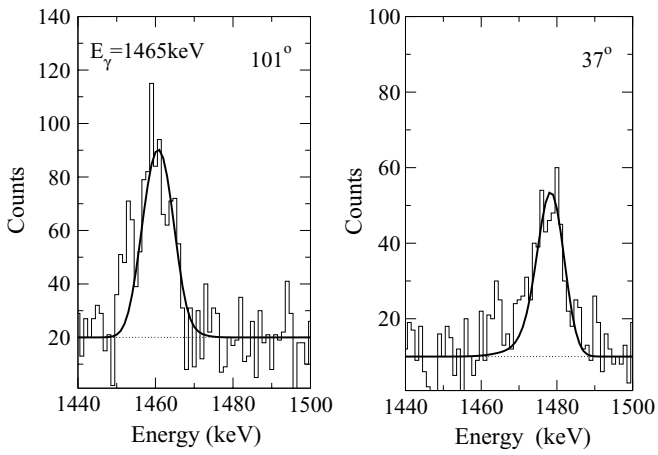

FIG. 7. Line-shape analysis for the $8^+ \rightarrow 7^+$ 1465-keV transition observed at 101° and 37° and gated on the 505-keV transition.

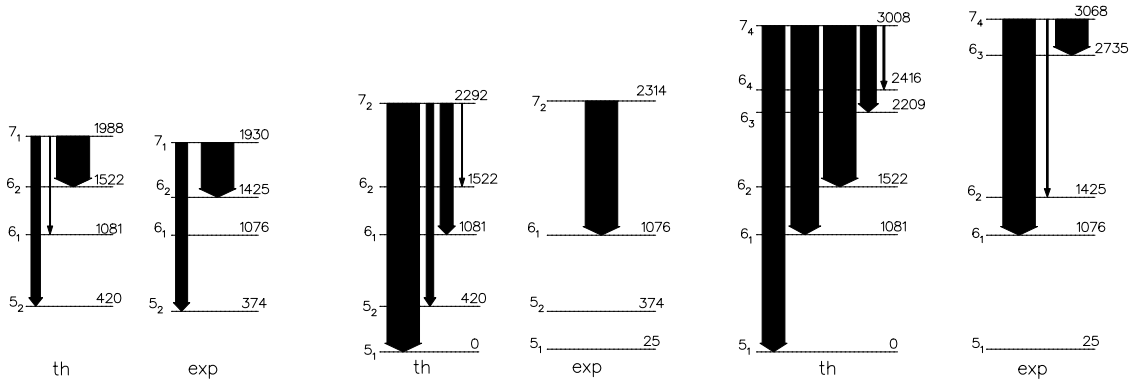

FIG. 8. Experimental and theoretical decay schemes for the excited states with spin 7.

shape or almost completely shifted γ lines, making possible the calculations of the transition probabilities reported in Table II. In Fig. 5, examples of line shapes are shown for the 1555- and 505-keV transitions, resulting in a lifetime value of $\tau = (0.40 \pm 0.04)$ ps for the 1930-keV state. Different line shapes for the 1050-and 1051-keV transitions, which belong to structures I and V, respectively, are shown in Fig. 6. It should be noted in Fig. 7 that the 1465-keV transition with a gate at 505 keV is shifted, characterizing a short lifetime $\tau = (0.10 \pm 0.06)$ ps for the 3394.6(12)-keV level.

V. DISCUSSION

One very early result of the nuclear shell model was an understanding of the origin of the $N = Z = 28$ magic number. The nucleus ^{56}Ni has the properties of a doubly magic inert core in the simplest spherical shell-model approach. One way to identify the impact of the core excitations on the structure of ^{58}Co is to compare the predictions of modern large-scale shell-model calculations with an effective interaction adjusted for the full pf shell, which includes different core excitations. To understand the observed structure of the ^{58}Co nucleus, spherical shell-model calculations have been performed with the code MSHELL [30]. For the description of the level structure of $A > 56$ nuclei, excitation of the ^{56}Ni core must be taken into account. We have considered the ^{56}Ni core, allowing up to eight particles to be excited from the $1f_{7/2}$ orbit to the $2p_{3/2}$, $1f_{5/2}$, and $2p_{1/2}$ orbitals. We have used the residual interaction named GXPF1, which is universal for the entire pf shell [5,10]. This interaction (195 two-body matrix elements and four single-particle energies) was determined partly from a fit to 699 experimental binding energies and level energies. This model space includes all four fp proton and neutron orbitals. The single-particle energies are taken to be −8.6240, −5.6793, −1.3829, and −4.1370 MeV for the $1f_{7/2}$, $2p_{3/2}$, $1f_{5/2}$, and $2p_{1/2}$ orbitals, respectively. The following effective charges and free g factors were used: $q^{\pi}_{\rm eff} = 1.23$, $q^{\nu}_{\rm eff} = 0.54$, $g^{\pi}_{s} = 5.586$, $g^{\nu}_{s} = -3.826$, $g^{\pi}_{l} = 1.0$, and $g^{\nu}_{l} = 0.0$.

To make a correspondence between a predicted level and a detected level means that both the level energies and the decay patterns should be in fair agreement, considering the branching ratios and $B(M1)$. An example of this identification for spin 7 levels is given in Fig. 8. The experimental 7_2 state has been associated in Table II with the theoretical 7_2 state; however, another possibility, as mentioned in Ref. [17], is the correspondence with the theoretical 7_3 state, which decays with 100% branching to the 6_1 with a calculated $B(M1) = 0.7\mu_N^2$. For the 7 yrast state it is possible to observe that the $7_1 \rightarrow 6_2$ and $7_1 \rightarrow 5_2$ transitions are well reproduced in energy and branching ratio; nevertheless, a low-intensity transition, $7_1 \rightarrow 6_1$, was predicted but not observed. The same is true for the $7_2 \rightarrow 6_1$ and $7_4 \rightarrow 6_1$ transitions, which are well reproduced but the other transitions were not well described. Even though the energy for the 7_3 level has been well reproduced, it is not possible to make the correspondence between the 7_3 experimental state and the calculated one. In this case, the final correspondence was obtained by also taking into account the $B(M1)$ values, which are more restrictive.

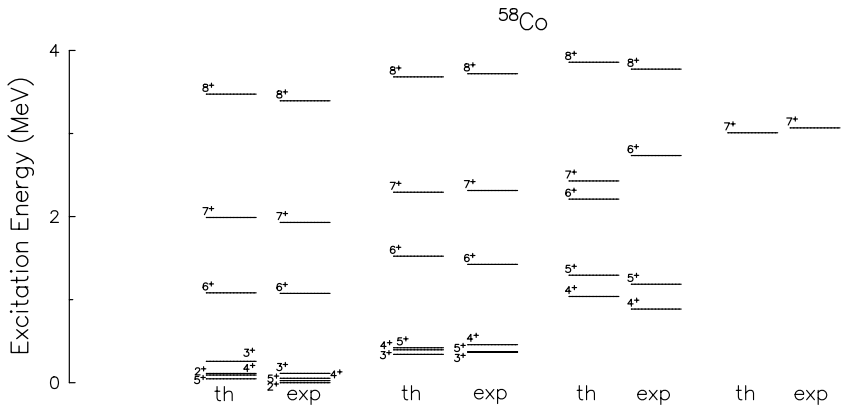

FIG. 9. Comparison between experimental and theoretical excited states in ^{58}Co.

TABLE III. Occupation numbers of the spherical orbitals for protons and neutrons used in the present shell-model calculations for the ^{58}Co nucleus.

State (J^π)	$\pi 1f_{7/2}$	$\pi 1p_{3/2}$	$\pi 1f_{5/2}$	$\pi 1p_{1/2}$	$\nu 1f_{7/2}$	$\nu 1p_{3/2}$	$\nu 1f_{5/2}$	$\nu 1p_{1/2}$
2_1^+	6.46	0.37	0.11	0.06	7.75	2.26	0.61	0.38
5_1^+	6.49	0.34	0.11	0.05	7.77	2.08	0.84	0.31
8_1^+	6.39	0.41	0.14	0.07	7.64	2.03	1.14	0.18
9_1^+	6.14	0.58	0.19	0.08	6.87	1.79	1.89	0.45

The shell model predicts some strong stretched $E2$ transitions, for example, $7_2 \rightarrow 5_1$ in Fig. 8. However, only one of these transitions has been observed in this work. The energies for measured and calculated excited states, energy transitions, spins and branching ratios, the experimental and theoretical lifetimes, and reduced $B(M1)$ and $B(E2)$ values are shown in Table II. The theoretical δ^2 values are smaller than 0.15 for all the transitions, except for those of 2361.0, 2710, and 1991.9 keV with $\delta^2 = 0.77$, 0.66, and 0.18, respectively. Most of the observed branching ratios are well reproduced by the MSHELL calculations. The exceptions are for the transitions depopulating the high-energy states. The lifetime for the 5_3^+ was already measured in Ref. [24] with a larger uncertainty. The $B(E2)$ for the $7_2 \rightarrow 5_1$ transition and most of the $B(M1)$ reduced values for the transitions depopulating the 5_3^+, 6_2^+, 7_1^+, and 8_1^+ levels are very well reproduced by the shell model. The experimental $B(M1)$ values for the transitions depopulating the 6_1^+ and 7_2^+ levels are reproduced within the same order of magnitude. In addition, the calculated $B(M1)$ values for the most intense transitions from the 4_2 and 5_2 states are within the experimental limits. The other experimental $B(M1)$ values are not well described with the model, showing differences up to three orders of magnitude, particularly for the high-energy states. The systematic trend for the experimental $M1$ rates to be less than those of theory may indicate the need for a renormalization of the $M1$ effective operator owing to higher-order configuration mixing and mesonic exchange currents. The low-lying levels of ^{58}Co, not observed in this work, were taken from Ref. [24]. For the four lowest levels, including the ground state, the largest disagreement is for the energy of the 3^+ level at 111.76(7) keV instead of the 257-keV prediction. About 25 transitions were considered in this comparison. In short, the assignment has been made on the basis of the level energies and the γ-decay pattern. In Fig. 9 a comparison of the experimental values with the calculations for the excited states of the odd-odd nucleus ^{58}Co are shown. Table III shows the particle occupation of the four orbitals included in the calculations for a few yrast states. The identified states presented wave functions with large configuration mixing, with the main configuration being $\pi f_{7/2}^{-1} \otimes \nu(p_{3/2}^2 f_{5/2}^1)$. The only exception is the calculated occupation number for the neutron orbital $f_{7/2}$ of the yrast 9^+ state, which differs from the occupation number for the yrast 8^+, explaining the absence of the $M1$ transition connecting these states (see Fig. 2). These calculations describe reasonably well the level scheme up to the third 8^+ state.

VI. CONCLUSIONS

The level scheme of the odd-odd ^{58}Co nucleus populated with a heavy-ion fusion-evaporation reaction was measured for the first time. The observed levels are grouped in five main structures with 46 new dipole transitions depopulating 36 new states. We have performed shell-model calculations for the states of ^{58}Co with the GXPF1 residual interaction, which is universal for the entire pf shell. From the theoretical point of view, it was necessary to use ^{40}Ca as the inert core in the valence space and consider up to eight particles in the full pf shell. The shell-model calculations reproduce reasonably well the experimental level scheme. It was possible to identify 19 excited states considering yrast states and 11 yrare states with $I \leqslant 8$ in three structures. We measured lifetimes of 14 levels; 11 of them were compared with values of the shell-model calculations with very good results for the $B(M1)$ values for the transitions depopulating the 4_2^+, 5_2^+, 5_3^+, 6_2^+, 7_1^+, and 8_1^+ states. All of the excited states are highly mixed with many particle-hole excitations. The predominant configuration is of one proton hole at $f_{7/2}$ coupled with two neutrons at $p_{3/2}$ and one neutron at the $f_{5/2}$ orbital. Wider ranging experimental information from the pf shell near the doubly magic core $N = Z = 28$ with the participation of several particle-hole pairs would help to complete a stringent test for the large-scale shell model.

ACKNOWLEDGMENTS

We thank the technical staff of the Pelletron Tandem Accelerator of the University of São Paulo for the maintenance of the equipment. This work was partially supported by the Fundação de Amparo à Pesquisa do Estado de São Paulo (FAPESP) and the Conselho Nacional de Desenvolvimento Científico e Tecnológico (CNPq), Brazil. B.A.B. acknowledges support from NSF Grant No. PHY-0244453.

[1] T. T. S. Kuo and G. E. Brown, Nucl. Phys. **A114**, 241 (1968).
[2] B. McGrory, B. H. Wildenthal, and E. C. Halbert, Phys. Rev. C **2**, 186 (1970).
[3] A. Poves and A. P. Zuker, Phys. Rep. **70**, 235 (1981).
[4] A. Poves, J. Sánchez-Solano, E. Caurier, and F. Nowacki, Nucl. Phys. **A694**, 157 (2001).
[5] M. Honma, T. Otsuka, B. A. Brown, and T. Mizusaki, Phys. Rev. C **65**, 061301(R) (2002).

[6] M. Palacz *et al.*, Nucl. Phys. **A627**, 162 (1997).
[7] S. M. Vicent *et al.*, Phys. Lett. **B437**, 264 (1998).
[8] D. Rudolph *et al.*, Eur. Phys. J. A **4**, 115 (1999).
[9] A. F. Lisetskiy *et al.*, Phys. Rev. C **68**, 034316 (2003).
[10] M. Honma, T. Otsuka, B. A. Brown, and T. Mizusaki, Phys. Rev. C **69**, 034335 (2004).
[11] T. Otsuka, M. Honma, and T. Mizusaki, Phys. Rev. Lett. **81**, 1588 (1998).
[12] O. L. Caballero *et al.*, Phys. Rev. C **67**, 024305 (2003).
[13] W. A. Richter *et al.*, Nucl. Phys. **A523**, 325 (1991).
[14] B. Elandsson and A. Marcinkowski, Nucl. Phys. **A146**, 43 (1970).
[15] A. C. Xenoulis and D. G. Sarantites, Nucl. Phys. **A170**, 369 (1971).
[16] B. J. Brunner *et al.*, Phys. Rev. C **11**, 1042 (1975).
[17] M. A. G. Silveira *et al.*, J. Phys. G: Nucl. Part. Phys. **31**, S1577 (2005).
[18] M. A. G. Silveira *et al.*, Braz. J. Phys. **35**, 821 (2006).
[19] J. A. Alcántara-Núñez *et al.*, Nucl. Instrum. Methods Phys. Res. A **497**, 429 (2003).
[20] R. V. Ribas *et al.*, Annual Report of the Nuclear Physics Department, IFUSP, São Paulo, Brazil, p. 63, 1996 (unpublished).
[21] W. T. Milner, *Holifield Heavy Ion Research Facility Computer Handbook*, Oak Ridge National Laboratory, 1987.
[22] D. Bazzacco and N. Marginean (private communication).
[23] D. Radford, Nucl. Instrum. Methods Phys. Res. A **361**, 297 (1995).
[24] M. R. Bhat, Nucl. Data Sheets **80**, 789 (1997).
[25] J. C. Wells and N. R. Jonhson, Report No. ORNL-6689 (1991).
[26] F. Brandolini and R. V. Ribas, Nucl. Instrum. Methods Phys. Res. A **417**, 150 (1998).
[27] J. Lindhard, M. Scharff, and H. E. Schiott, Mat. Fys. Medd. Dan. Vid. Selsk. **33** (14), 1 (1963).
[28] W. M. Currie, Nucl. Instrum. Methods **73**, 173 (1969).
[29] L. C. Northcliffe and R. F. Schilling, Nucl. Data Tables A **7**, 233 (1970).
[30] T. Mizusaki, RIKEN Accel. Prog. Rep. **33**, 14 (2000).